Efficient Multisignal 2–4-GHz Power Amplifier With Power Tracking

Maxwell Robert Duffy, *Student Member, IEEE*, Gregor Lasser, *Member, IEEE*, Morten Olavsbråten, *Member, IEEE*, Eric Berry, and Zoya Popović, *Fellow, IEEE*

Abstract—The goal of the work presented in this paper is to demonstrate an efficient method of amplifying multiple concurrent signals over a large bandwidth using a supply modulation approach. A single-stage octave bandwidth (2–4 GHz) power amplifier (PA) with greater than 10-W output power and drain efficiency ranging from 48%–60% is presented. The amplifier is tested with several reduced-bandwidth supply modulation trajectories that are constructed as an even-termed power series of a 10-MHz LTE signal envelope. A greater than 30% point increase in η_D is achieved while maintaining less than -45-dB ACPR with digital predistortion (DPD). Two 10-MHz LTE signals with 800-MHz spacing are then amplified using a similar bandwidth-reduction technique. A greater than 20% point increase in η_D is seen with an improvement in linearity through the use of multidimensional DPD. The method presented here can be extended to more than two concurrent signals of arbitrary spacing for a PA with large RF bandwidth.

Index Terms—Broadband, carrier aggregation, efficiency, GaN, power amplifiers (PAs), supply modulation.

I. INTRODUCTION

THE trend to replace multiple power amplifiers (PAs) with a single component has resulted in increased interest in multiband and broadband PAs for carrier aggregation of high peak-to-average power ratio (PAPR) signals [1]. Several approaches for improving backoff efficiency over a broad bandwidth have been reported, including increased-bandwidth Doherty [2], [3] and other load-modulated PAs [4], [5]. These PAs require multiple amplifiers and are generally designed for a specific signal type. On the other hand, supply modulation, often referred to as envelope tracking, can be more flexible and achieve increased average efficiency for a single-ended efficient PA [6]. Multiple methods for single-ended GaN broadband PA s with harmonic tuning have been demonstrated, including a class-J [7], continuous class-F [8], load–pull
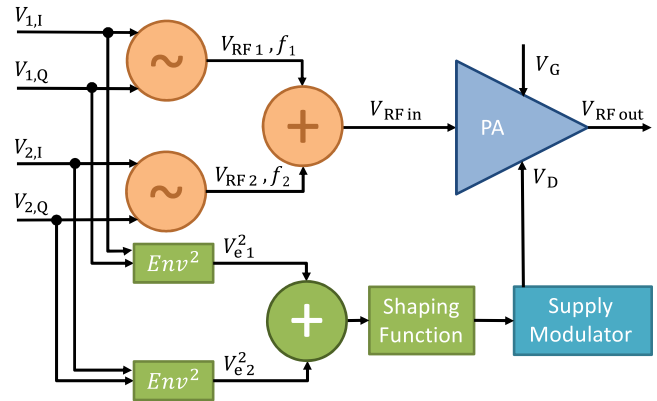
Fig. 1. Block diagram of a concurrent dual-signal transmitter with supply modulation. The shaping functions, or trajectories, are expressed in terms of the square of the envelope, or more generally a power series with even powers of the envelope. The two signals V_{RF1} and V_{RF2} are at frequencies f_1 and f_2 that are arbitrarily spaced within the PA RF operating band.

optimized [9], and stepped-impedance-matched PA [10]. In all cases, the output impedance at the fundamental is matched for efficiency over the entire band, while the harmonics are terminated in various manners, and the device is biased in class AB or B. For maximum efficiency, the saturation level results in the need to linearize the PA.

Due to the very large instantaneous bandwidths associated with carrier aggregation, continuous envelope tracking is impractical. For example, if switching power supplies are used for envelope modulation, due to the inverse relationship between efficiency and switching speed [11], the overall transmitter efficiency becomes limited as the instantaneous signal bandwidth increases. The relationship between the supply voltage, V_D and the RF input voltage across a constant load, V_{in}, is referred to as a shaping function, or trajectory. In order to maintain the efficiency of the tracker, the trajectory can be modified through slew-rate reduction [12]–[14] or the use of discrete supply modulation [15]–[17]. When multiple simultaneous signals are amplified, the resulting overall signal bandwidth increases as a function of signal spacing, making efficient tracking difficult. A possible solution is to track the sum of envelopes (SoE), rather than the envelope of the composite signal, as presented in [18]–[21]. This results in a trajectory that can be tracked with a slower and more efficient supply modulator. The goal of this paper presented here is to demonstrate that an increase in average efficiency is possible while maintaining linearity.

Fig. 2. Solid lines: output impedance targets of the fundamental (2–4 GHz), second (4–8 GHz), and third harmonic (6–12 GHz) from simulated load–pull. Dashed lines: realized impedances of output matching network. Because the second harmonic has a higher impact on efficiency than the third, it takes precedence where the two overlap.
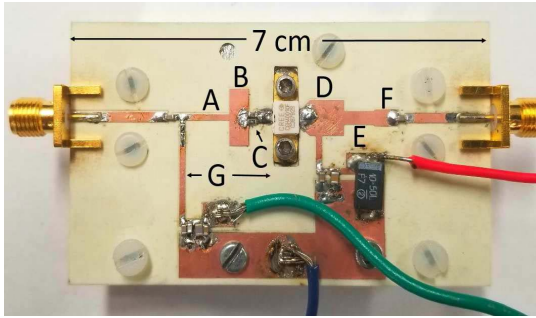
Fig. 3. Fabricated 2–4-GHz PA based on a Cree (Wolfspeed) CGH40010F GaN on SiC HEMT with stepped-impedance matching line segments of A-66 Ω, B-15 Ω, C-gate stability network, D-21 Ω, E-41 Ω, F-36 Ω, G-1.5 cm. The substrate is a 0.762 mm Rogers 4835. To enable supply modulation, all bypass capacitors on the drain bias line except for a 10 pF one are removed.

A method for overcoming the limitations of past slew rate reduction techniques is proposed in [22]–[25]. The method, referred to as power envelope tracking, or just power tracking (PT), only uses the even terms of a power series of the signal envelope (see Fig. 1). Neither early trajectory designs, reviewed in, e.g., [26], or more recent ones, e.g., [27] and [28], aim to reduce envelope bandwidth. In the work presented here, the PT approach is investigated by optimizing different metrics, such as peak power-added efficiency (PAE), flat gain and a trade between linearity and efficiency. First, we present the results for a single signal, followed by an extension to two widely separated signals. We show that the PT method used in conjunction with average SoE tracking [29] results in a band-limited trajectory for multisignal envelope tracking.

To demonstrate the approach, a high-efficiency octave bandwidth (2–4 GHz) GaN high PA, based on the design originally presented in [30] with two widely spaced signals, is expanded to a supply-modulated transmitter. The PA is first characterized statically for amplitude and phase variation over input drive for trajectory design. Several different trajectories for PT are designed and discussed in terms of bandwidth reduction and linearity. The amplifier is tested using a 10-MHz LTE signal with supply modulation, and results with and without
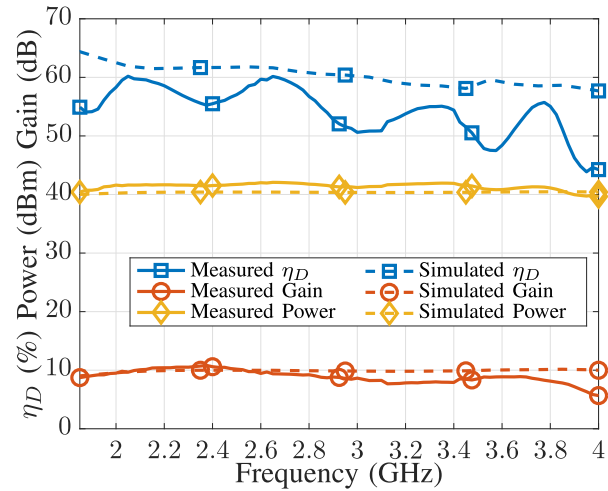
Fig. 4. Amplifier large signal performance at saturation over frequency. Solid curve: measured results. Dashed curve: simulated results.

digital predistortion (DPD) are compared. Multisignal efficient amplification is next shown using two 10-MHz LTE signals, 800 MHz apart, using a new supply modulation trajectory, and efficiency improvement is demonstrated for a linearized PA.

II. BROADBAND AMPLIFIER DESIGN

The hybrid PA uses a Cree (Wolfspeed) CGH40010F GaN on SiC HEMT and the broadband design is based on simulated load–pull for maximum efficiency over 2–12 GHz, which takes into account up to the third harmonic of the highest frequency in the band. The sensitivity to the impedance at the fundamental frequency is examined to inform required matching for flat efficiency across the band. The upper frequency range from 3.5–4 GHz is most affected by impedance variations. In the lower frequency range (2–3 GHz), the PAE reaches over 80% in load–pull simulations but was reduced in order to achieve uniform gain response across the octave bandwidth.

To achieve broadband matching, short transmission line sections that approximate lumped elements over the band are implemented, similar to the stepped-impedance networks in [10], [31]. The final topology is generated by constraining the number of transmission line sections to three at the output, and two at the input, with a goal of simplicity and reduced footprint. The range of microstrip line impedances is constrained between 15 and 70 Ω. The ideal terminations found from load–pull and the realized output matching network impedances are shown in Fig. 2. A parallel RC network is added in series at the gate terminal in the input match to ensure stability. The fabricated amplifier is shown in Fig. 3, and the continuous wave (CW) measured performance is summarized in Fig. 4. In the operating range of 1.9–3.8 GHz, the amplifier maintains a drain efficiency greater than 45%, output power over 40 dBm, and large signal gain of 8–10 dB at 28-V drain bias and 200-mA quiescent drain current.

III. TRAJECTORY DESIGN FOR SINGLE-SIGNAL AND DUAL-SIGNAL SUPPLY MODULATION

To achieve high efficiency in an envelope-tracking PA, a specific trajectory $V_D(V_{in})$ is selected and will be different
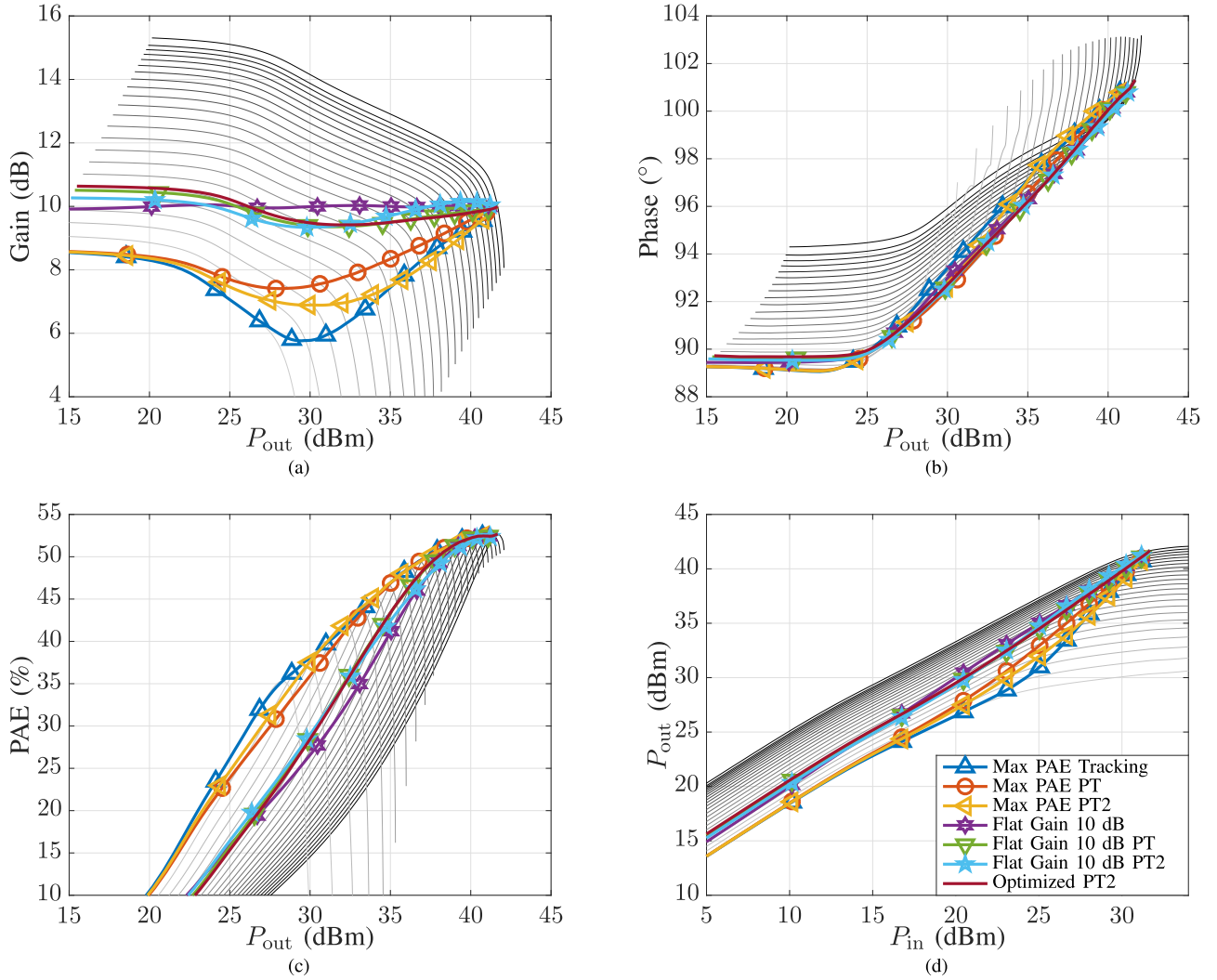
Fig. 5.   Measured (a) gain amplitude, (b) phase, and (c) PAE versus output power. (d) Compression curves of the PA from Fig. 3 shown in gray lines as a function of drain voltage (6–28 V in 1 V steps). Seven trajectories are superimposed onto static measurements. Darker lines: higher drain voltages.

from, e.g., a flat gain trajectory. Because switching power supply modulators degrade in efficiency as switching frequency increases, a trajectory that minimizes envelope bandwidth is used to improve composite transmitter efficiency. Traditional methods of trajectory design aim to create an accurate tracking function but do not minimize the envelope bandwidth of the signal [27], [28]. Other methods of trajectory design aim to reduce the required slew rate (or envelope bandwidth) while sacrificing the accuracy of the tracking function and eliminating the clear $V_D(V_{in})$ function [12]–[14].

A. Signal Power Tracking

A method for overcoming the limitations of previous slew-rate reduction techniques is proposed in [22]–[25]. The method, referred to as PT, fits the desired $V_D(V_{in})$ trajectory by approximating it as a first- or second-order power series of the envelope. This method uses only even exponents of the series, resulting in a supply voltage that is proportional to the power, square of the power, etc. of the signal. This, in turn, results in a tracking bandwidth limited to integer multiples of the signal bandwidth. For example, for a quadratic

series, it reduces to the signal bandwidth, while for a fourth power of V_{in}, or second-order PT (PT2), the required tracking bandwidth is twice that of the signal.

The envelope, V_e, of the RF signal can be used to generate a tracking trajectory as

$$V_e = \sqrt{V_I^2 + V_Q^2}$$
$$B_e = \infty \tag{1}$$

Due to the presence of the square root function, the resulting envelope bandwidth, B_e, in general, is infinite, though there are some cases such as an AM signal where the bandwidth is finite. The increased bandwidth is explained mathematically by looking at the infinite series expansions of a square root function

$$\sqrt{x} = \sum_{n=1}^{\infty} \frac{(-1)^n (-1+x)^n \left(\frac{1}{2}\right)_n}{n!}$$
$$\approx a_0 + a_1 x^1 + a_2 x^2 + a_3 x^3 \ldots \tag{2}$$

Raising a signal to the nth power increases the signal bandwidth by a factor of n, and taking the square root of that
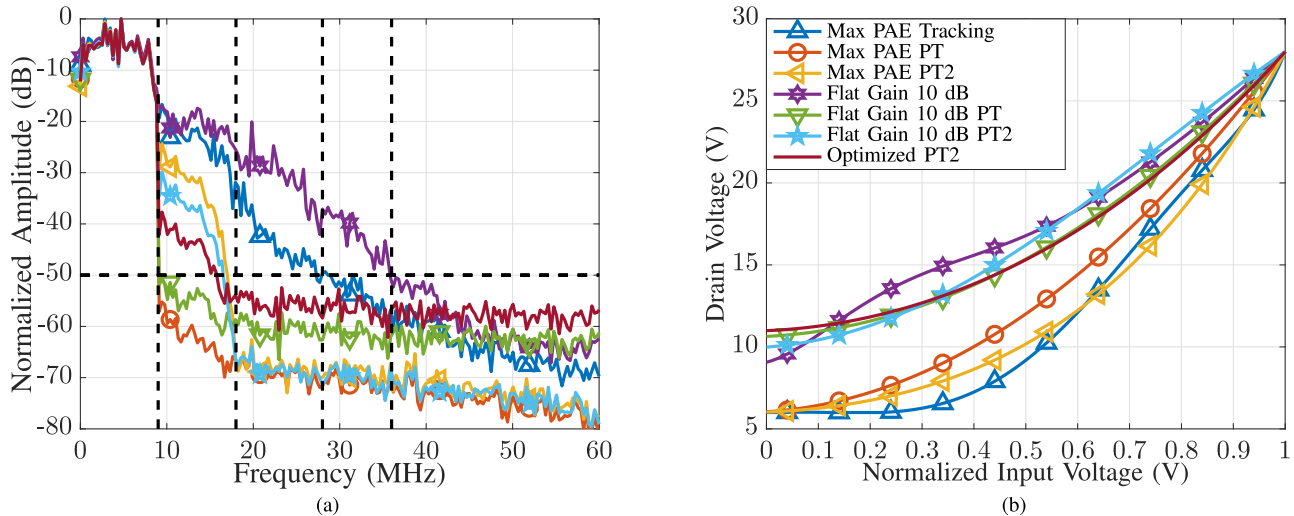
Fig. 6. (a) Simulated normalized amplitude versus frequency for the four synthesized trajectories. Note that the PT trajectory results in a 9-MHz bandwidth, while PT2 gives 18 MHz. In contrast, the traditional envelope trajectories extend to 28–37 MHz. (b) Drain supply voltage versus normalized input voltage for the seven trajectories. The PT and PT2 trajectories are smoother, as they use fewer terms.

function results in an infinite sum and therefore an infinite bandwidth. The coefficients a_n drop with higher values of n due to the $(1/n!)$ term. The higher frequency components can be truncated when developing a trajectory, as their low values do not have an effect on the performance.

Now, it is perhaps clearer why PT, based on even powers of V_e, reduces the required tracking bandwidth by removing the square root function, thus creating a band-limited trajectory with a bandwidth matching that of the RF signal, B_{RF}

$$V_e^2 = V_I^2 + V_Q^2$$
$$V_{PT} = a_0 + a_2 \cdot V_e^2$$
$$B_e = B_{RF}. \tag{3}$$

This function can be extended to higher orders for more accurate tracking. Second-order PT is given by

$$V_{PT2} = a_0 + a_2 \cdot V_e^2 + a_4 \cdot V_e^4$$
$$B_e = 2 \cdot B_{RF} \tag{4}$$

where the coefficients (a_0, a_2, and a_4) can be selected to fit a trajectory that optimizes a given metric.

B. Single-Signal Trajectory Design

Two trajectories are developed to compare the performance of PT to a "traditional" trajectory, one for flat gain and one for maximum PAE. The former sets the PA gain to a constant value as the input voltage varies, while the latter follows the peak PAE points for each of the drain supply voltage level PAE(P_{in}) curves. The results from this analysis at 2.1 GHz are shown in Fig. 5. Measurements are performed using a power calibrated VNA with an external test set; this extracts static AM/AM and AM/phase modulation data in a fully calibrated environment. The drain voltage is swept in 1-V steps from 6 to 28 V.

Fig. 5 shows the response of the PA with the seven trajectories calculated from the static measurements. The traditional trajectories better track the $V_D(V_{in})$ characteristic they are selected to follow. The maximum PAE (max-PAE) tracking

TABLE I
COMPARISON OF DIFFERENT TRAJECTORIES

Trajectory	Pout	Gain	η_D	PAE	NMSE	ACPR
Static V_D	33.6	13	24.7	23.4	-16.8	-31.9
max-PAE	30.8	6.7	51.6	40.5	-9.08	-26.5
max-PAE PT	32.3	8.1	49.9	42.2	-13.4	-31.5
max-PAE PT2	31.4	7.2	50.6	41	-9.2	-31.5
flat-gain 10dB	34.2	10	44	39.6	-31.8	-38.3
flat-gain PT	33.7	9.5	45.4	40.3	-24.4	-36.6
flat-gain PT2	33.9	9.7	45.2	40.4	-27.4	-35.3
Optimized PT2	33.7	9.5	45.2	40.2	-24.3	-36.9

PT: Power Tracking, PT2: 2nd order PT
Pout(dBm), Gain(dB), PAE(%), η_D(%), NMSE(dB), ACPR(dBc)

function is able to hit the peaks of the PAE (P_{in}) for each voltage level, while the flat gain function results in a perfectly flat gain. The PT cases approximate these ideal trajectories. It should be noted that all of these trajectories increase phase distortion from ~3° with a constant 28 V to ~10° with a varying supply.

The seven trajectories and their corresponding spectra are shown in Fig. 6. The spectral benefit of PT can be seen in Fig. 6(a): the 28–37-MHz bandwidth required for standard envelope tracking of a 10-MHz LTE signal (including two 0.5 MHz guard bands) is reduced to 9 MHz, where bandwidth is defined at frequencies where the spectrum amplitude drops by 50 dB (excluding the dc offset). Fig. 6(b) shows that the max-PAE PT trajectory is a shallower version of the traditional max-PAE trajectory. A higher order function better approximates the shape, as seen with the PT2 case. The traditional flat-gain trajectory is a kinked line which also cannot be approximated by a first-order PT. The PT2 case offers a closer approximation but still does not perfectly track the original case, which implies that the AM–AM distortion is increased.

The performance of the amplifier is analyzed, as a first-order approximation, by assuming a memoryless model and applying the gain and phase trajectories developed from the static measurements to a 10-MHz LTE signal. The results of this analysis are given in Table I. Note that for all supply
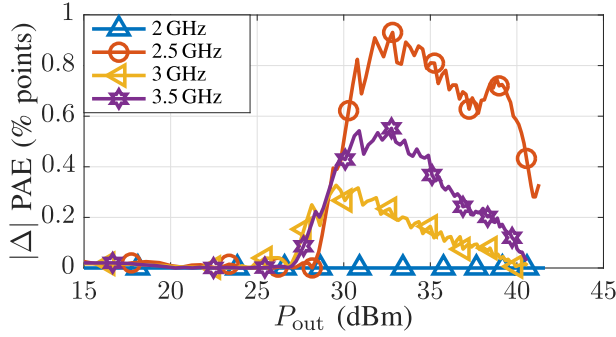
Fig. 7. Variation in PAE at several (2.5, 3, and 3.5 GHz) frequencies for the max-PAE trajectory created at each respective frequency point versus the one created at 2 GHz and applied at the other frequency points. Applying the trajectory designed at 2 GHz to the other frequencies will result in a less than 1% point variation in PAE.

Fig. 8. Variation in Gain at several (2.5, 3, and 3.5 GHz) frequencies applying the flat-gain 10-dB trajectory made for 2 GHz. Note that even though the gains do not stay constant at 10 dB, gain variation for the power sweeps is ±0.5 dB.

modulated cases, the PAE is approximately the same at 40%. For the max-PAE tracking cases, the gain of the transmitted signal is reduced compared to the static case, and there is a 3–7-dB decrease in normalized mean square error (NMSE), calculated as

$$\text{NMSE(dB)} = 10 \cdot \log 10 \frac{\sum_n |x(n) - y(n)|^2}{\sum_n |x(n)|^2} \tag{5}$$

where x is the input and y is the output.

The flat-gain cases offer a better compromise than the max-PAE case since the PAE remains the same while the linearity is improved. An "optimized PT2" trajectory was created by maximizing PAE and the linearity metric signal to total distortion ratio (STDR), presented [32]. The optimization consisted of identifying coefficients that improve both STDR and PAE simultaneously, equal weighting was ascribed to both metrics.

If the amplifier is operated at another frequency, a lookup table of PT coefficients can be created for each operating point. The effect of using the ideal (non-PT) trajectories developed for a signal at 2 GHz and applied to different frequencies is examined in Fig. 7 for the max-PAE case and Fig. 8 for the flat-gain 10-dB case. As seen from Fig. 7, using the max-PAE trajectory developed at 2 GHz at different frequencies will have a small (less than 1% point) effect on PAE as a function of output power. Applying the flat-gain trajectory developed for 2 GHz to other frequencies results in an output with flat gain (±0.5 dB) as a function of P_{out} but does not result in the target gain, as shown in Fig. 8.

C. Two-Signal Trajectory Design

In carrier aggregation, an amplifier is driven by multiple signals across its operational bandwidth. Supply modulation for efficiency enhancement will differ in this case compared to a single signal since the total signal bandwidth and PAPR are increased. Generating a trajectory for two signals can be done as in (1), where the I and Q components of the composite signal are considered. However, doing this would result in a tracking bandwidth of at least $5 \cdot (f_2 - f_1)$ for a two-signal case. Due to the inverse relationship between switching supply speed and efficiency, as signal spacing increases, this technique becomes less practical.
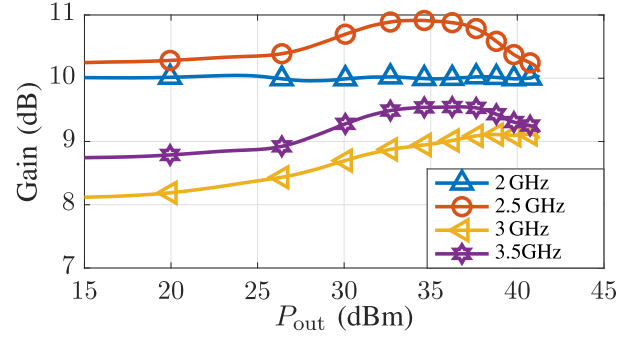
A method for overcoming this is called sum of envelopes (SoE) tracking. Performing SoE tracking reduces the bandwidth requirements for the supply modulator to that of the largest individual signal bandwidth. There are two main SoE approaches: peak SoE [20], [33], [34] and average SoE [29]. In peak SoE tracking, the peaks of the signals are tracked

$$V_{\hat{S}e} = \Sigma_i^N V_{e_i} \tag{6}$$

where V_{e_i} is the envelope of one of the N multiple signals. The alternative, average SoE tracking is defined as

$$V_{\overline{S}e} = \sqrt{\Sigma_i^N V_{e_i}^2} \tag{7}$$

Both methods provide an improvement in efficiency, though average SoE is shown in [29] to provide a larger improvement.

The techniques discussed earlier for PT are easily applicable to (7). Expanding this equation for two signals gives

$$V_{\overline{S}e} = \sqrt{\left(\sqrt{V_{1,I}^2 + V_{1,Q}^2}\right)^2 + \left(\sqrt{V_{2,I}^2 + V_{2,Q}^2}\right)^2}. \tag{8}$$

This is simplified to

$$V_{\overline{S}e} = \sqrt{V_{1,I}^2 + V_{1,Q}^2 + V_{2,I}^2 + V_{2,Q}^2}. \tag{9}$$

The function in (9) can then be used with (3) to produce a PT trajectory that is band limited to the signal bandwidth, or with (4) to twice the signal bandwidth. This method can be used with average SoE tracking since squaring the absolute value function eliminates the square root function from the envelope. If this method were used with peak SoE tracking, the square root of the calculation of the V_{e_i} would not be removed, and the resulting function would not be band limited.

Trajectories are designed for five cases of two 10-MHz signals separated by 50 MHz: envelope tracking, peak SoE tracking, average SoE tracking, average SoE PT, and average SoE PT2. A 50-MHz spacing is used for this simulation to allow easier visualization of the concepts discussed in this paper, later testing is done with an 800-MHz spacing. The resulting spectra are given in Fig. 9. The PT trajectories band limit the required tracking spectrum to the signal bandwidth for PT and twice the signal bandwidth for PT2. The average SoE and peak SoE trajectories have tracking bandwidths
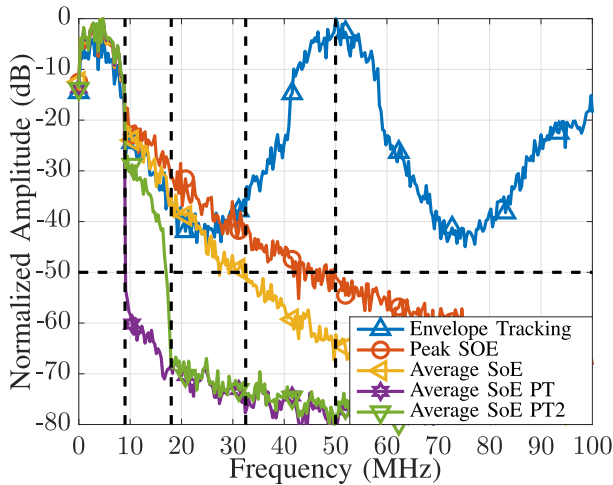
Fig. 9. Normalized spectra of five trajectories for multisignal envelope tracking. Two 10-MHz LTE signals are used with a 50-MHz spacing.
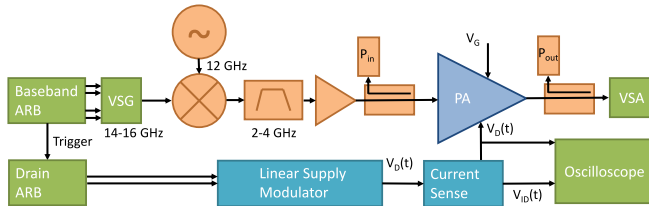
Fig. 10. Block diagram of measurement setup for validating trajectory design applied to the 2-4-GHz GaN PA from Fig. 3.

of 32 and 50 MHz, respectively. Note that for a 50-MHz signal spacing, traditional envelope tracking would require a tracking bandwidth exceeding 500 MHz.

IV. Measurement Setup and Calibration

A test bench developed to validate the tracking theory described earlier is shown in Fig. 10. The signals are generated with a Keysight E8267D Vector Signal Generator (VSG) in conjunction with an N8241A Arbitrary Waveform Generator (AWG) with a sampling rate of 1.25 Gs/s. This configuration enables the generation signals with up to 1-GHz bandwidth; however, at lower carrier frequencies (<3.2 GHz), the bandwidth that the VSG can generate without distortion is reduced to 130 MHz. To overcome this, the VSG operates in X-band, and a mixer is used to downconvert the signal to the band of interest (2–4 GHz). The signal is then received at both the input and output of the DUT using an N9030A Vector Signal Analyzer which has a maximum receive bandwidth of 160 MHz. Measurements at the input of the DUT are done to evaluate the linearity of the test bench itself.

The envelope signal is generated with an identical AWG to that used for signal generation. The two AWGs use the same clock and one is triggered off the other to ensure there is no drift between them. Envelope measurements are performed using a 5-Gs/s oscilloscope. The oscilloscope is set to match the sampling rate of the AWG's (1.25 Gs/s). An N2876A low-capacitance RF probe is used for voltage measurements, while an N2819A high-frequency differential probe is used for ac current measurements.
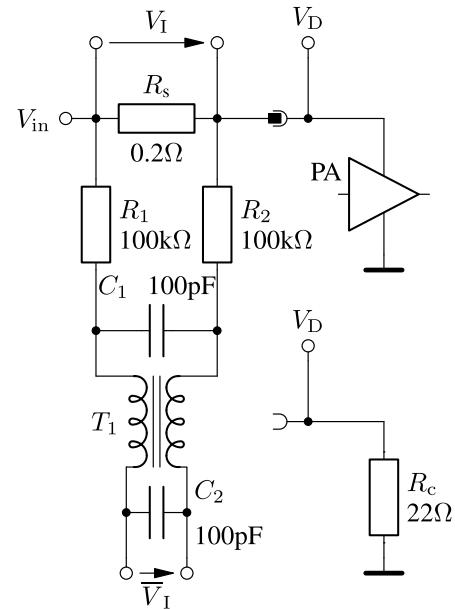
Fig. 11. Drain current calibration and measurement. The left part of the circuit is the current sense circuitry that can be connected either to the amplifier board (top right) or the calibration board (bottom right).

Accurate measurements of envelope voltage and current are required when characterizing a supply-modulated transmitter, in order to determine the P_{dc} and therefore the efficiency of the device. To illustrate the importance of accurate P_{dc} measurements, consider the case of using just the dc component of the envelope to calculate efficiency. For the 2–4-GHz PA, this will result in an efficiency measurement that is 5 percentage points higher than the correct value. The current is therefore measured separately for ac and dc components.

1) Calibration of AC Current Measurements: Current measurements are taken across the $R_s = 0.2$ Ω resistor at the output of the linear tracker, Fig. 11. Due to the interconnect used to probe the circuit and the differential probe's frequency dependence, a calibration needs to be performed. A "calibration board" is created with the same interconnects and shape as the amplifier board, but loaded with a $R_c = 22$ Ω 1206 SMD resistor in place of the bias line shunt capacitor, and with the RF transistor removed, shown in Fig. 11. Measurements are then performed with a linear tracker transmitting a 100-MHz multicarrier noiselike signal. With the voltage measured across the load and the value of the resistor known, the current through the load is determined.

These two signals, the ideal current, and the differential voltage V_I can then be converted into the frequency domain and divided to create an equalization function that converts the measured differential voltage to the actual current. Due to the small value of the sense resistor R_s, the resulting equalization function is noisy and a moving average smoothing function is applied to the frequency response, shown in Fig. 13(a). The equalization function is shown with and without smoothing in the frequency domain. The smoothed version is converted into the time domain, truncated and convolved with the raw differential voltage measurements to give the corrected current. The effect of this filter function can be seen in Fig. 13(b) in the time domain current measurements.
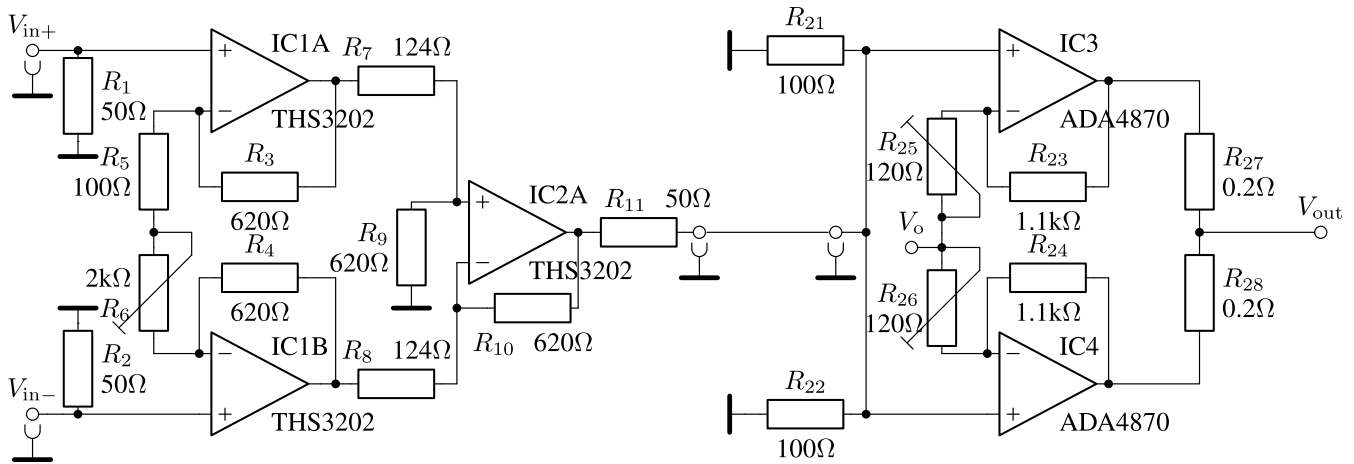
Fig. 12. Simplified circuit diagram of the linear tracker. The left side shows the differential-to-single-ended converter, the right side contains the power op-amps which create the drain voltage. The interconnect enables either single-ended or differential operation of the supply modulator.
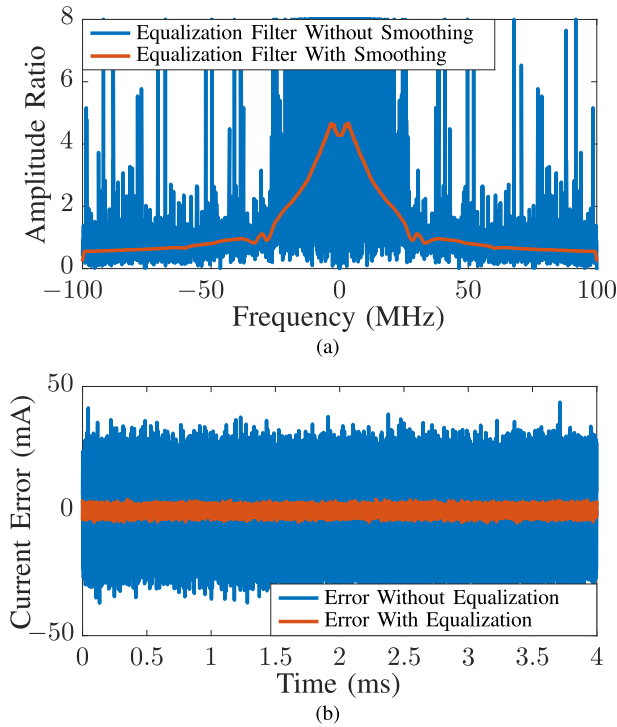
Fig. 13. (a) Equalization filter response generated to correct the parasitics in the current measurement setup. (b) Effect of the equalization on the 4-ms noiselike signal used for calibration.

2) Calibration of DC Current Measurements: For validation of the differential probe for dc current measurements, we used a voltmeter to probe the dc component of the input current and apply this as an offset to the oscilloscope reading. This is done because we noticed that the differential probe zero reading is susceptible to variation with probe movement and thermal drift. An *RC* network is placed around the sense resistor which is also being used by the differential probe, Fig. 11. The values of $R_{1,2}$ and C_1 are set such that the time constant of the network is much greater than the signal length. A common mode choke T_1 further suppresses any interference from the envelope signal, followed by an additional capacitor C_2. This voltage V_1 is probed by a high impedance (1 GΩ) voltage

meter which measures the voltage drop across resistor R_s. Loading the circuit with the "calibration board" and calculating the current through the resistor determines a factor which converts the measured voltage drop $\overline{V}_I$ to the dc component of the current.

To further validate the measurement accuracy, we recharacterized the PA with a CW 2.1-GHz signal and saw an excellent agreement with the PAE data obtained by the VNA bench.

3) Time Alignment of Envelope and RF Path: A time alignment is performed using a 10-MHz band-limited noise signal which looks similar to a pulse in the time domain. A trajectory with a range from 6 to 28 V is designed to match the settings of the linear tracker. The delay of the envelope path is adjusted until a minimum NMSE is found [35], [36], corresponding to the maximum power and efficiency point of the amplifier. With the AWG used in the setup, a potential 6.4-ns resolution is possible for the signal delay.

4) Linear Tracker: The linear tracker is a modification of the design from [20] and uses the Analog Devices ADA4870 Current Feedback operational amplifier, chosen for its high current drive (1 A), slew rate (2500 V/μs), and bandwidth ($>$50 MHz). A schematic of the tracker is shown in Fig. 12. For the peak PA drain current of 1.1 A, two op-amps are connected in parallel. The output voltage is centered around 17 V using the offset voltage V_o. The slew rate, SR, specification of 2500 V/μs suggests that the circuit is capable of distortion-free tracking of signals with bandwidths up to 18 MHz for an output voltage swing of 6–28 V (22 V_{pp}). The maximum bandwidth capabilities of the tracker can be determined as

$$f = \frac{2 \cdot \pi \cdot V_{pp}}{SR}. \tag{10}$$

Two 200-mΩ series resistors, R_{27} and R_{28}, are added to each amplifier output to compensate for slight gain mismatches between IC3 and IC4, and help stabilize the op-amps from capacitive loading under various biasing conditions of the RFPA. An additional 200-mΩ resistor between the output of the linear tracker and the PA drain line is used in the current sensing circuit (see Fig. 11). The gain is boosted by a differential to single-ended stage with three
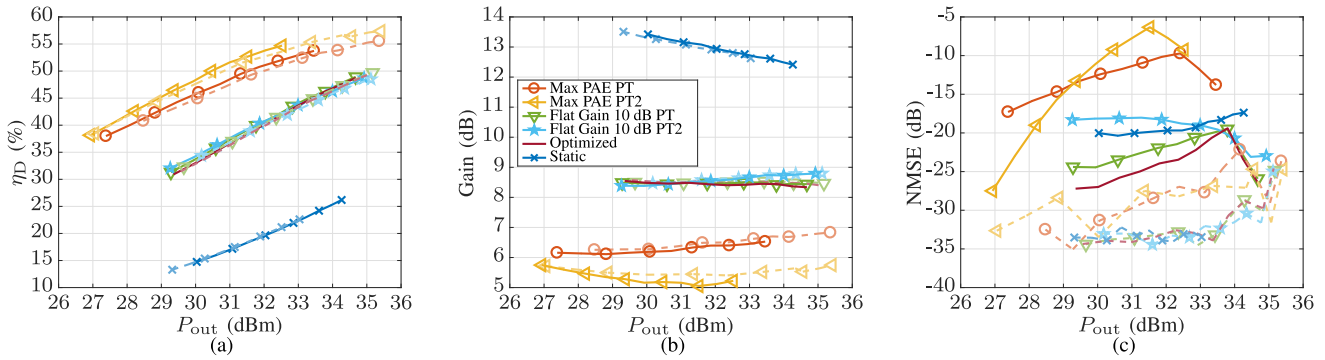
Fig. 14. Measured (a) η_D, (b) gain, and (c) NMSE versus output power for six different cases, with (faded dashed lines) and without (solid lines) DPD for a single 10-MHz signal at 2.1 GHz.

TABLE II
COMPARISON OF DIFFERENT TRAJECTORIES AT 30- AND 33-dBm OUTPUT POWER

Trajectory	Pout (dBm)	Gain (dB)	PAE (%)	η_D(%)	NMSE (dB)	ACPR$_L$ (dBc)	ACPR$_U$ (dBc)
Static V_D	30	13.4	14.1	14.7	-20	-35.6	-35.4
w/ DPD	29.8	**13.4**	13.7	14.4	**-33.5**	**-49.2**	**-50.4**
max-PAE PT	30.1	6.19	**34.9**	46	-12.4	-30	-30.9
w/ DPD	30.1	6.27	34.3	44.9	**-31.3**	**-45.6**	-43.2
max-PAE PT2	29.9	5.16	33.4	**48.1**	-11.1	-32.9	-36.2
w/ DPD	30	5.43	34.1	47.7	**-33.5**	**-47.4**	**-49.2**
flat-gain PT	29.9	8.47	28.8	33.5	-24.5	-36.9	-37.3
w/ DPD	29.7	8.5	27.7	32.3	**-33**	**-47**	**-49**
flat-gain PT2	29.9	8.38	29.1	34	-18.1	-32.7	-33.6
w/ DPD	30.2	8.47	29.5	34.4	**-33.1**	**-47.5**	**-49.5**
Optimized PT2	30	8.48	28.4	33.1	-27	-38.3	-38.8
w/ DPD	30.3	8.51	29	33.8	**-33.9**	**-50.8**	**-49.8**
Static V_D	32.9	**12.8**	20.8	22	-19.3	-37	-37.2
w/ DPD	33	12.6	21.4	22.6	**-33.5**	**-49.7**	**-51.1**
max-PAE PT	32.9	6.45	40.8	52.8	-11.7	-28.1	-28.5
w/ DPD	33.1	6.62	**41**	52.4	-27.7	-42.5	-40.6
max-PAE PT2	32.5	5.22	38.3	54.7	-9.3	-27.9	-29.3
w/ DPD	33.4	5.52	39.8	**55.3**	-26.9	-43.6	-41.6
flat-gain PT	32.8	8.5	37.4	43.5	-20.6	-33.6	-34.5
w/ DPD	32.9	8.51	37.1	43.2	**-34.5**	**-50.3**	**-49.7**
flat-gain PT2	33	8.67	37.8	43.7	-19	-30.6	-31.1
w/ DPD	33.1	8.67	37.4	43.2	**-32**	-41.2	-42.1
Optimized PT2	32.9	8.42	37	43.2	-22.2	-34.5	-36.3
w/ DPD	32.9	8.48	36.9	43	**-33**	**-50.1**	**-49.6**

PT: Power Tracking, PT2: 2nd ord. PT

THS3202 op-amps configured as an instrumentation amplifier, which are drawn on the left side of Fig. 12. This allows for a lower gain setting of the power stages (IC3 and IC4), which results in a lower output impedance of the tracker, favorable for envelope tracking. No equalization is done on the linear tracker itself, since it is confirmed by measurement that the error between the tracker and AWG output is below the noise floor.

V. MEASUREMENT RESULTS

A. Single-Signal Results

Linearity testing of the PA is performed using a 10-MHz LTE downlink signal with PAPR = 8.5 dB generated in MATLAB. Measurements are first done with the original signal, and subsequently with DPD applied. The PA is linearized using the model shown in [37] with a seventh-order polynomial and seven memory taps—the long-term stability of the DPD. The DPD is first applied to the signal and then the predistorted signal is used to generate an updated

trajectory for the supply modulator, this maintains the same $V_D(V_{in})$ characteristic with or without DPD.

The PA output power is stepped in 0.5-dB increments from 27–35 dBm. At each power level, the DPD algorithm generates a new signal. The DPD algorithm linearizes to the peak output power level achieved in the characterization. It does not additionally adapt the input power to match the characterization output power. The trajectories are designed from Fig. 6(b) for the output powers shown in Table I. If the PA is overdriven and the voltage expected to swing above 28 V, we clip the trajectory that expands the bandwidth, though it is possible to redesign the trajectory with clipping in mind. If, on the other hand, the PA is underdriven and the peak voltage does not reach 28 V, the trajectory remains the same but the peak voltage is reduced. Measured results at 2.1 GHz are shown in Fig. 14, where the drain efficiency, gain, and NMSE are presented for 12 different cases (6 without DPD). The DPD provides improvement, particularly, at lower power levels and for trajectories that flatten gain. It is interesting to observe that with the addition of DPD, the average output power of the max-PAE case increases. This can be attributed
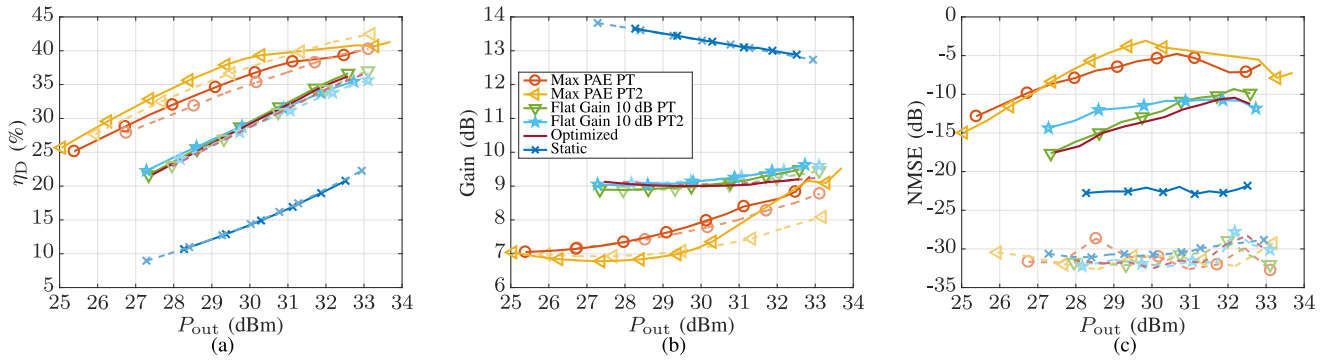
Fig. 15.   Measured (a) η_D, (b) gain, and (c) NMSE versus output power for six different cases, with (faded dashed lines) and without (solid lines) DPD for two 10-MHz signals centered at 2.15 and 2.95 GHz (800 MHz apart).

TABLE III

COMPARISON OF DIFFERENT TRAJECTORIES FOR TWO SIGNAL OPERATION

Trajectory	Pout (dBm)	Gain (dB)	PAE (%)	η_D (%)	NMSE$_1$ (dB)	ACPR$_1$ (dBc)	NMSE$_2$ (dB)	ACPR$_2$ (dBc)
Static V_D	29.9	13.3	13.3	13.9	-22.1	-34	-24.2	-33.7
w/ DPD	30	13.3	13.7	14.4	**-31.9**	-44.8	**-30.7**	**-45.9**
max-PAE PT	30.1	7.98	30.9	36.8	-8.05	-26.3	-7.91	-27.3
w/ DPD	30.2	7.78	29.4	35.3	**-31**	**-47**	**-31.7**	**-48**
max-PAE PT2	29.8	7.14	**31.3**	**38.8**	-5.57	-26	-6.91	-27.1
w/ DPD	30.4	7.25	31.2	38.4	**-30.9**	-41.4	**-31.7**	-41.5
flat-gain PT	29.7	8.99	25.1	28.8	-14.8	-32.7	-13.6	-33.1
w/ DPD	30.1	8.98	25.4	29.1	**-32.5**	**-45.4**	**-32.1**	**-45.7**
flat-gain PT2	29.8	9.13	25.3	28.8	-13.5	-31.1	-12	-31.8
w/ DPD	29.7	9.15	24.6	28	**-32.9**	**-46.3**	**-31.9**	**-46.6**
Optimized PT2	29.8	9	25	28.6	-16.3	-33.4	-14.2	-33.4
w/ DPD	30	9.05	25.2	28.8	**-32.5**	**-46.2**	**-32.8**	**-46.7**
Static V_D	32.5	12.9	19.7	20.8	-21.8	-34.6	-23.8	-32
w/ DPD	33	12.4	20.9	22.2	-29.4	-40	-28.7	-42.6
max-PAE PT	32.9	9.29	35.3	40	-10.8	-24.7	-6.14	-25.2
w/ DPD	33.1	8.77	34.9	40.2	**-32.8**	**-47.5**	**-32.9**	**-46.9**
max-PAE PT2	32.8	9.15	35.8	40.8	-10	-23.2	-5.53	-23.7
w/ DPD	33.2	8.09	35.9	42.5	**-30.8**	-38.7	-29.3	-38.5
flat-gain PT	32.6	9.49	32.5	36.7	-12.7	-29.8	-10.2	-30
w/ DPD	33.1	9.45	32.8	37	**-32.8**	**-46**	**-32**	**-45.6**
flat-gain PT2	32.7	9.63	31.6	35.5	-12.5	-28.5	-10.7	-29.6
w/ DPD	33.1	9.6	31.8	35.7	**-32.6**	**-46.8**	**-30.1**	**-47.3**
Optimized PT2	32.6	9.21	31.9	36.2	-11.4	-29.6	-10.7	-31.1
w/ DPD	33	9.24	32.3	36.6	**-30.3**	**-46.7**	**-31.3**	**-48.4**

PT: Power Tracking, PT2: 2nd ord. PT

to the expansive gain characteristic of the amplifier, as shown in Fig. 5(a) when tracked for the max-PAE PT/PT2 cases. Linearizing the amplifier in these cases requires an input signal that has a higher average power than the signal without DPD, resulting in a higher output power.

Selected results of these measurements are displayed in Table II for 30-dBm average output power (top) and 33-dBm average output power when the PA is compressed (bottom). The following conclusions can be made.

1) Using a static supply provides the highest gain with the lowest efficiency and a competitive linearity.
2) The PT and PT2 max-PAE cases provide the highest PAE and η_D but these trajectories also have the lowest gain and worse raw linearity.
3) The flat-gain cases and the optimized PT2 case for minimized NSME and maximized PAE provide very similar performance in terms of gain and efficiency. Though the gain is designed to be 10 dB from the static measurements, this is reduced by 1–1.5 dB in the dynamic results. This reduction is a well-known

phenomenon in GaN related to trapping effect [38] and was previously reported on in [39] and [40]. Dual-pulse characterization of GaN devices and PAs has shown the same effect [41]. This is also observed in the gain performance of the other trajectories.

4) The optimized PT2 trajectory does improve linearity over the two flat-gain cases and is seen to have better performance even than the static bias case for some measures of linearity.
5) The trends we see are similar to those calculated in Table I. The differences between these results are related to the simplicity of the memoryless model and the use of static measurements to model an amplifier operating in a dynamic fashion.
6) Supply modulation increases the drain efficiency by more than 30% points with a greater than 20% point improvement in PAE. At the lower drive level, P_{out} = 30 dBm, in conjunction with DPD, and for all but one trajectory, max-PAE PT, achieve less than −45-dB ACPR for both upper and lower channels.
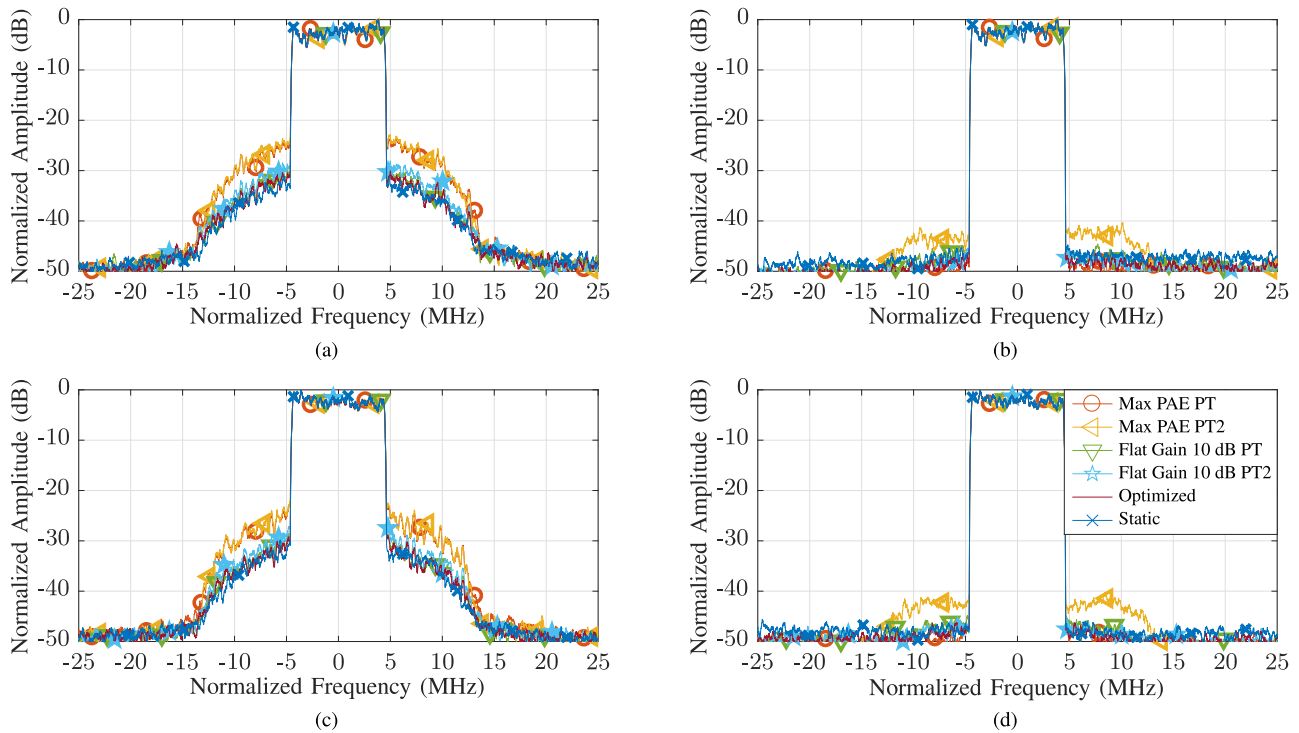
Fig. 16. Measured spectra for $P_{out} = 30$ dBm with two signals. (a) Lower band. (b) Lower band with DPD. (c) Upper band. (d) Upper band with DPD.

For all but the max-PAE PT case, a NMSE < -30 dB is realized.

7) At the higher output power level, $P_{out} = 33$ dBm, a reduction in linearity can be observed for all but two cases. The flat gain and optimized PT2 cases both still show less than -45-dBc ACPR for both the upper and lower channel and an NMSE of less than -30 dB. A higher order memory polynomial might benefit the other cases at a higher power level for achieving ACPR < -45 dBc.

B. Multiple Signal Results

The amplifier is tested with two concurrent 10-MHz LTE signals at 2.15 and 2.95 GHz for an 800-MHz total signal spacing. DPD is performed using the algorithm presented in [42], using seven memory taps and seventh-order polynomial for each cross term. As the tracking trajectory changes (and if the signal spacing changes), the DPD coefficients need to be updated. A power sweep is performed for the same trajectories as in the single-signal case. The power sweep results are shown in Fig. 15.

The selected results of these measurements are summarized in Table III. The two ACPR columns show the worse of the two channels. Supply modulation offers a 14%–23% point improvement in drain efficiency and 12%–16% percentage points in PAE, compared to the static supply case. The trends in gain are similar to those seen with one signal, though there is a 0.5-dB higher gain for the flat-gain and optimized PT2 trajectories, and a gain expansion with increasing drive level for the two max-PAE cases. At the lower drive level ($P_{out} = 30$ dBm) in conjunction with DPD, all but one

trajectory, max-PAE PT2, achieve ACPR < -45 dBc for both upper and lower channels. For all but the max-PAE PT2 case, a NMSE < -30 dB is realized. Spectra measurements for the lower drive level case are shown in Fig. 16. Similar conclusions can be drawn at the higher output power level ($P_{out} = 33$ dBm).

VI. CONCLUSION

In summary, this paper demonstrates an efficient method of amplifying multiple concurrent signals over a large bandwidth using a supply modulation approach. An efficient broadband hybrid PA based on a Cree (Wolfspeed) CGH40010F GaN on SiC HEMT achieves octave bandwidth (2–4 GHz) using stepped-impedance compact matching at the fundamental, second and third harmonic frequencies. The amplifier operates with 45%–60% peak drain efficiency, 10-dB saturated gain, and >10-W peak output power.

The amplifier is first tested using a single 10-MHz signal with several reduced-bandwidth supply modulation trajectories that are constructed as an even-termed power series of a 10-MHz LTE signal envelope. With this PT approach, a greater than 30% point increase in η_D is achieved while maintaining less than -45-dB ACPR with DPD. Two 10-MHz LTE signals with 800-MHz spacing are then amplified using a similar bandwidth-reduction technique. A greater than 20% point increase in η_D is seen with an improvement in linearity through the use of multidimensional DPD, and several orders of magnitude tracking bandwidth reduction. The method presented here can be extended to more than two concurrent signals of arbitrary spacing for a PA with large RF bandwidth.

The efficiency improvement results presented here are shown for the PA without taking into account the

instrumentation linear tracker efficiency. Previous work has demonstrated efficient 100-MHz switching GaN trackers, e.g., [11] with 90% efficiency at 10-W output power. To obtain composite PAE, this efficiency multiplies the PA efficiency, still resulting in overall substantial efficiency improvement. The focus of the paper is to show that sum-of-envelope PT significantly improves PA efficiency for two widely spaced signals with potentially dynamic and arbitrary spacing, and with a tracking bandwidth that is approximately that of a single signal.

REFERENCES

[1] S. A. Bassam, W. Chen, M. Helaoui, and F. M. Ghannouchi, "Transmitter architecture for CA: Carrier aggregation in LTE-Advanced systems," *IEEE Microw. Mag.*, vol. 14, no. 5, pp. 78–86, Jul./Aug. 2013.

[2] M. N. A. Abadi, H. Golestaneh, H. Sarbishaei, and S. Boumaiza, "Doherty power amplifier with extended bandwidth and improved linearizability under carrier-aggregated signal stimuli," *IEEE Microw. Wireless Compon. Lett.*, vol. 26, no. 5, pp. 358–360, May 2016.

[3] R. Darraji, D. Bhaskar, T. Sharma, M. Helaoui, P. Mousavi, and F. M. Ghannouchi, "Generalized theory and design methodology of wideband Doherty amplifiers applied to the realization of an octave-bandwidth prototype," *IEEE Trans. Microw. Theory Techn.*, vol. 65, no. 8, pp. 3014–3023, Aug. 2017.

[4] D. J. Shepphard, J. Powell, and S. C. Cripps, "An efficient broadband reconfigurable power amplifier using active load modulation," *IEEE Microw. Wireless Compon. Lett.*, vol. 26, no. 6, pp. 443–445, Jun. 2016.

[5] P. H. Pednekar and T. W. Barton, "RF-input load modulated balanced amplifier," in *IEEE MTT-S Int. Microw. Symp. Dig.*, Jun. 2017, pp. 1730–1733.

[6] P. Asbeck and Z. Popovic, "ET comes of age: Envelope tracking for higher-efficiency power amplifiers," *IEEE Microw. Mag.*, vol. 17, no. 3, pp. 16–25, Mar. 2016.

[7] P. Wright, J. Lees, J. Benedikt, P. J. Tasker, and S. C. Cripps, "A methodology for realizing high efficiency class-J in a linear and broadband PA," *IEEE Trans. Microw. Theory Techn.*, vol. 57, no. 12, pp. 3196–3204, Dec. 2009.

[8] H. Huang, B. Zhang, C. Yu, J. Gao, Y. Wu, and Y. Liu, "Design of multioctave bandwidth power amplifier based on resistive second-harmonic impedance continuous class-F," *IEEE Microw. Wireless Compon. Lett.*, vol. 27, no. 9, pp. 830–832, Sep. 2017.

[9] P. Saad, C. Fager, H. Cao, H. Zirath, and K. Andersson, "Design of a highly efficient 2–4-GHz octave bandwidth GaN-HEMT power amplifier," *IEEE Trans. Microw. Theory Techn.*, vol. 58, no. 7, pp. 1677–1685, Jul. 2010.

[10] J. Xia, X.-W. Zhu, and L. Zhang, "A linearized 2–3.5 GHz highly efficient harmonic-tuned power amplifier exploiting stepped-impedance filtering matching network," *IEEE Microw. Wireless Compon. Lett.*, vol. 24, no. 9, pp. 602–604, Sep. 2014.

[11] Y. Zhang, M. Rodríguez, and D. Maksimović, "100 MHz, 20 V, 90% efficient synchronous buck converter with integrated gate driver," in *Proc. IEEE Energy Convers. Congr. Expo. (ECCE)*, Sep. 2014, pp. 3664–3671.

[12] J. Jeong, D. F. Kimball, M. Kwak, C. Hsia, P. Draxler, and P. M. Asbeck, "Wideband envelope tracking power amplifiers with reduced bandwidth power supply waveforms and adaptive digital predistortion techniques," *IEEE Trans. Microw. Theory Techn.*, vol. 57, no. 12, pp. 3307–3314, Dec. 2009.

[13] G. Montoro, P. L. Gilabert, P. Vizarreta, and E. Bertran, "Slew-rate limited envelopes for driving envelope tracking amplifiers," in *Proc. IEEE Top. Conf. Power Amplif. Wireless Radio Appl.*, Jan. 2011, pp. 17–20.

[14] P. L. Gilabert, G. Montoro, and P. Vizarreta, "Slew-rate and efficiency trade-off in slow envelope tracking power amplifiers," in *Proc. 7th German Microw. Conf.*, Mar. 2012, pp. 1–4.

[15] G. Lasser, M. Duffy, J. Vance, and Z. Popović, "Discrete-level envelope tracking for broadband noise-like signals," in *IEEE MTT-S Int. Microw. Symp. Dig.*, Jun. 2017, pp. 1942–1945.

[16] C. Florian, T. Cappello, R. P. Paganelli, D. Niessen, and F. Filicori, "Envelope tracking of an RF high power amplifier with an 8-level digitally controlled GaN-on-Si supply modulator," *IEEE Trans. Microw. Theory Techn.*, vol. 63, no. 8, pp. 2589–2602, Aug. 2015.

[17] N. Wolff, W. Heinrich, and O. Bengtsson, "Highly efficient 1.8-GHz amplifier with 120-MHz class-G supply modulation," *IEEE Trans. Microw. Theory Techn.*, vol. 65, no. 12, pp. 5223–5230, Dec. 2017.

[18] F. M. Ghannouchi, A. K. Kwan, M. Younes, and W. Chen, "DSP techniques for linearity and efficiency enhancement of multi-band envelope tracking transmitters," in *Proc. Asia–Pacific Microw. Conf.*, Nov. 2014, pp. 1082–1084.

[19] Y. Lin, C. Quindroit, H. Jang, and P. Roblin, "3-D Fourier series based digital predistortion technique for concurrent dual-band envelope tracking with reduced envelope bandwidth," *IEEE Trans. Microw. Theory Techn.*, vol. 63, no. 9, pp. 2764–2775, Sep. 2015.

[20] M. R. Duffy et al., "Bandwidth-reduced supply modulation of a high-efficiency X-band GaN MMIC PA for multiple wideband signals," in *IEEE MTT-S Int. Microw. Symp. Dig.*, Jun. 2017, pp. 1850–1853.

[21] P. L. Gilabert and G. Montoro, "3-D distributed memory polynomial behavioral model for concurrent dual-band envelope tracking power amplifier linearization," *IEEE Trans. Microw. Theory Techn.*, vol. 63, no. 2, pp. 638–648, Feb. 2015.

[22] P. Midya et al., "Method, device, phone and base station for providing envelope-following for variable envelope radio frequency signals," U.S. Patent 6 141 541, Oct. 31, 2000.

[23] P. Midya, K. Haddad, L. Connell, S. Bergstedt, and B. Roeckner, "Tracking power converter for supply modulation of RF power amplifiers," in *Proc. IEEE 32nd Annu. Power Electron. Spec. Conf.*, vol. 3, Jun. 2001, pp. 1540–1545.

[24] M. Olavsbråten, D. Gecan, M. R. Duffy, G. Lasser, and Z. Popovic, "Efficiency enhancement and linearization of GaN PAs using reduced-bandwidth supply modulation," in *Proc. 47th Eur. Microw. Conf. (EuMC)*, Oct. 2017, pp. 456–459.

[25] M. Olavsbråten and D. Gecan, "Bandwidth reduction for supply modulated RF PAs using power envelope tracking," *IEEE Microw. Wireless Compon. Lett.*, vol. 27, no. 4, pp. 374–376, Apr. 2017.

[26] J. Hoversten and Z. Popović, "System considerations for efficient and linear supply modulated RF transmitters," in *Proc. IEEE 12th Workshop Control Model. Power Electron. (COMPEL)*, Jun. 2010, pp. 1–8.

[27] B. Kim et al., "Push the envelope: Design concepts for envelope-tracking power amplifiers," *IEEE Microw. Mag.*, vol. 14, no. 3, pp. 68–81, May 2013.

[28] N. Giovannelli, T. Vlasits, A. Cidronali, and G. Manes, "Efficiency and linearity enhancements with envelope shaping control in wideband envelope tracking GaAs PA," in *Proc. Workshop Integr. Nonlinear Microw. Millimetre-Wave Circuits*, Apr. 2011, pp. 1–4.

[29] Y. Lin, H. Jang, C. Quindroit, N. Naraharisetti, and P. Roblin, "New supply modulation optimization methodology for concurrent dual band envelope tracking power amplifier," in *Proc. WAMICON*, Jun. 2014, pp. 1–4.

[30] M. R. Duffy, E. Berry, G. Lasser, and Z. Popović, "An efficient linearized octave-bandwidth power amplifier for carrier aggregation," in *IEEE MTT-S Int. Microw. Symp. Dig.*, Jun. 2018, pp. 327–346.

[31] M. Olavsbråten, T. Mathiesen, and E. Berry, "Design of an efficient wideband (1–5 GHz) 10 W PA in GaN technology using harmonic tuning," in *Proc. IEEE 18th Wireless Microw. Technol. Conf. (WAMICON)*, Apr. 2017, pp. 1–5.

[32] D. Gecan, K. M. Gjertsen, and M. Olavsbråten, "Novel metric describing total nonlinearity of power amplifier with a corresponding figure of merit for linearity evaluation and optimization," *IEEE Microw. Wireless Compon. Lett.*, vol. 27, no. 1, pp. 85–87, Jan. 2017.

[33] H. Sarbishaei, B. Fehri, Y. Hu, and S. Boumaiza, "Dual-band Volterra series digital pre-distortion for envelope tracking power amplifiers," *IEEE Microw. Wireless Compon. Lett.*, vol. 24, no. 6, pp. 430–432, Jun. 2014.

[34] P. L. Gilabert, G. Montoro, D. López, and J. A. García, "3D digital predistortion for dual-band envelope tracking power amplifiers," in *Proc. Asia–Pacific Microw. Conf. (APMC)*, Nov. 2013, pp. 734–736.

[35] J. Hoversten et al., "Codesign of PA, supply, and signal processing for linear supply-modulated RF transmitters," *IEEE Trans. Microw. Theory Techn.*, vol. 60, no. 6, pp. 2010–2020, Jun. 2012.

[36] F. Wang, A. H. Yang, D. F. Kimball, L. E. Larson, and P. M. Asbeck, "Design of wide-bandwidth envelope-tracking power amplifiers for OFDM applications," *IEEE Trans. Microw. Theory Techn.*, vol. 53, no. 4, pp. 1244–1255, Apr. 2005.

[37] L. Ding et al., "A robust digital baseband predistorter constructed using memory polynomials," *IEEE Trans. Commun.*, vol. 52, no. 1, pp. 159–165, Jan. 2004.

[38] S. C. Binari *et al.*, "Trapping effects and microwave power performance in AlGaN/GaN HEMTs," *IEEE Trans. Electron Devices*, vol. 48, no. 3, pp. 465–471, Mar. 2001.

[39] J. C. Pedro, L. C. Nunes, and P. M. Cabral, "Soft compression and the origins of nonlinear behavior of gan hemts," in *Proc. 9th Eur. Microw. Integr. Circuit Conf.*, Oct. 2014, pp. 353–356.

[40] N. Wolff, W. Heinrich, and O. Bengtsson, "Challenges in the design of wideband GaN-HEMT based class-G RF-power amplifiers," in *Proc. German Microw. Conf. (GeMiC)*, Mar. 2016, pp. 189–192.

[41] C. Florian, T. Cappello, A. Santarelli, D. Niessen, F. Filicori, and Z. Popović, "A prepulsing technique for the characterization of GaN power amplifiers with dynamic supply under controlled thermal and trapping states," *IEEE Trans. Microw. Theory Techn.*, vol. 65, no. 12, pp. 5046–5062, Dec. 2017.

[42] S. A. Bassam, M. Helaoui, and F. M. Ghannouchi, "2-D digital predistortion (2-D-DPD) architecture for concurrent dual-band transmitters," *IEEE Trans. Microw. Theory Techn.*, vol. 59, no. 10, pp. 2547–2553, Oct. 2011.

Eric Berry received the B.S. and M.S. degrees in electrical engineering from the University of Colorado at Boulder, Boulder, CO, USA, in 2016 and 2017, respectively.

Since 2017, he has been with Lockheed Martin Space Systems, Littleton, CO, USA, where he is involved in designing of RF hardware for satellite communications.

Maxwell Robert Duffy (S'16) received the B.S. degree in electrical engineering from The College of New Jersey, Ewing, NJ, USA, in 2015, and the M.S. degree in electrical engineering from the University of Colorado at Boulder, Boulder, CO, USA, in 2017, where he is currently pursuing the Ph.D. degree.

From 2013 to 2015, he was a Test Engineer with Linearizer Technology, Hamilton, NJ, USA, where he was involved in supporting the production of analog predistortion linearizers. His current research interests include efficient power amplifier design and architectures.

Gregor Lasser (S'09–M'15) received the Dipl.-Ing. and Dr.Techn. degrees (Hons.) in electrical engineering from the Vienna University of Technology, Vienna, Austria, in 2008 and 2014, respectively.

Since 2017, he has been an Assistant Research Professor with the University of Colorado at Boulder, Boulder, CO, USA, where he is involved in broadband supply-modulated power amplifiers and compact intelligent antenna systems.

Dr. Lasser has served as the Vice Chair for the IEEE Denver Joint AP-S/MTT Section since 2016. He was the recipient of the EEEfCOM Innovation Award (Second Place) in 2008 for the RFID testbed developed during his diploma thesis, the Faculty Award of the Faculty of Electrical Engineering and Information Technology, Vienna University of Technology for the presentation of his doctoral dissertation entitled "Passive RFID for Automotive Sensor Applications," and the Best Paper Award of IEEE WAMICON in 2017 for his work on analog predistortion of GaN power amplifiers.

Morten Olavsbråten (S'94–M'03) received the M.Sc. degree in electrical engineering from the Norwegian Institute of Technology, Trondheim, Norway, in 1993, and the Ph.D. degree in electrical engineering from the Norwegian University of Science and Technology (NTNU), Trondheim, in 2003.

He was a Manager with the department, where he was involved in several research projects funded by Norwegian Research Council, NoE TARGET, and Cost 0803 RFCSET. Since 2003, he has been a Full-Time Associate Professor with the Department of Electronics and Telecommunications, NTNU, where he was the Head of the Radio Systems Group from 2009 to 2015. From 2016 to 2017, he was a Sabbatical Visitor with Zoya Popović's group at the University of Colorado at Boulder, Boulder, CO, USA. His teaching experience covers more than five different courses at graduate and undergraduate level, including circuit design, radio systems, microwave integrated circuits, and nonlinear microwave components. He has supervised, on average, two Ph.D. candidates and five master candidates each year. He is currently the Deputy of Education with the Department of Electronic Systems, NTNU. His current research interests include several fields of RF and microwaves, such as transistor modeling, power amplifier (PA) modeling and design, PA architectures, microwave measurements techniques including time domain waveform measurements.

Zoya Popović (S'86–M'90–SM'99–F'02) received the Dipl.-Ing. degree from the University of Belgrade, Belgrade, Serbia, and the Ph.D. degree from California Institute of Technology, Pasadena, CA, USA.

From 2001 to 2003, she was a Visiting Professor with the Technical University of Munich, Munich, Germany. In 2014, she was a Visiting Professor with the National School of Aeronautics and Space, Toulouse, France. Since 2018, she has been a Chair of Excellence with Carlos III University of Madrid, Getafe, Spain. She has graduated 58 Ph.D. students and currently advises 14 doctoral students. She is currently a Distinguished Professor and the Lockheed Martin Endowed Chair of Electrical Engineering with the University of Colorado at Boulder, Boulder, CO, USA. Her current research interests are in high-efficiency power amplifiers and transmitters, microwave and millimeter-wave high-performance circuits for communications and radar, medical applications of microwaves, and wireless powering.

Dr. Popović was a recipient of two IEEE MTT Microwave Prizes for best journal papers, the White House NSF Presidential Faculty Fellow Award, the URSI Issac Koga Gold Medal, the ASEE/HP Terman Medal, and the German Humboldt Research Award. She was elected as a Foreign Member of the Serbian Academy of Sciences and Arts in 2006. She was named the IEEE MTT-S Distinguished Educator in 2013 and the University of Colorado Distinguished Research Lecturer in 2015.